Hao et al. Nanoscale Research Letters (2017) 12:562
DOI 10.1186/s11671-017-2334-z

Nanoscale Research Letters

NANO EXPRESS Open Access

Large Lateral Photovoltaic Effect in MoS_2/GaAs Heterojunction

Lanzhong Hao[1,2*], Yunjie Liu[1], Zhide Han[1], Zhijie Xu[1] and Jun Zhu[2]

Abstract

Molybdenum disulfide (MoS_2) nanoscaled films are deposited on GaAs substrates via magnetron sputtering technique, and MoS_2/GaAs heterojunctions are fabricated. The lateral photovoltaic effect (LPE) of the fabricated MoS_2/GaAs heterojunctions is investigated. The results show that a large LPE can be obtained in the MoS_2/*n*-GaAs heterojunction. The LPE exhibits a linear dependence on the position of the laser illumination and the considerably high sensitivity of 416.4 mV mm^{-1}. This sensitivity is much larger than the values in other reported MoS_2-based devices. Comparatively, the LPE in the MoS_2/*p*-GaAs heterojunction is much weaker. The mechanisms to the LPE are unveiled by constructing the energy-band alignment of the MoS_2/GaAs heterojunctions. The excellent LPE characteristics make MoS_2 films combined with GaAs semiconductors promising candidates for the application of high-performance position-sensitive detectors.

Keywords: MoS_2, GaAs, Photovoltaic, Heterojunction, Interface

Background

Due to its excellent properties, molybdenum disulfide (MoS_2) is being investigated as one typical kind of two-dimensional materials to develop next-generation microelectronic devices and optoelectronic devices [1–5]. Unlike graphene, MoS_2 has obvious band gap and its band gap decreases with increasing layer numbers [6]. The presence of the obvious band gap allows the fabrication of the MoS_2 transistors with an on/off ratio exceeding 10^8 and the photodetectors with high responsivity [7, 8]. Recently, MoS_2 combined with other semiconductors has attracted much interest, such as GaAs, Si, and GaN [9–13]. These designed heterostructures supply feasible technical route for MoS_2-based materials to develop practically applicable optoelectronic devices. Among all these bulk semiconductors, GaAs has a suitable direct band gap of ~ 1.42 eV and high electron mobility (~ 8000 cm^2 V^{-1} s^{-1}). Lin et al. fabricated MoS_2/GaAs solar cells with a power conversion efficiency over 9.03% [9]. Further, Xu et al. reported a MoS_2/GaAs self-driven photodetector with the extremely high detectivity of 3.5×10^{13} Jones [10]. In previous reports, the studies on MoS_2/GaAs heterostructures have been mainly focused on the application in the area of solar cells and photodetectors. However, the MoS_2/GaAs as a position-sensitive detector (PSD) based on the lateral photovoltaic effect (LPE) has been reported rarely. Different from the ordinary longitudinal photovoltaic effect, the LPE originates from the lateral diffusion and recombination of the photon-generated carriers in the inversion layer at the interface [14–18]. In the LPE effect, a lateral photovoltage (LPV) can be obtained and it changes linearly with the laser spot position on the active region of the device surface. These characteristics make LPE very useful in developing high-performance PSDs and have been studied widely in the area of robotics, biomedical applications, process control, position information systems, and so on.

In this work, MoS_2 thin films with different thickness are deposited on the surface of *n*-/*p*-GaAs substrates via magnetron sputtering technique. A large LPE is observed in the fabricated MoS_2/*n*-GaAs heterojunction, and the sensitivity reached 416.4 mV mm^{-1}. Our results further show that the LPE exhibits obvious dependence on the carrier types of the GaAs substrates and the thickness of the MoS_2 films. Through the construction

* Correspondence: haolanzhong@upc.edu.cn
[1]College of Science, China University of Petroleum, Qingdao 266580, Shandong, People's Republic of China
[2]State Key Laboratory of Electronic Thin Films and Integrated Devices, University of Electronic Science and Technology of China, Chengdu 610054, People's Republic of China

of the energy-band alignment at the interface, the mechanisms to the LPE in the devices are proposed.

Methods

MoS_2 thin films were deposited on (100)-oriented GaAs substrates using the DC magnetron sputtering technique. The MoS_2 powders (purity, ~ 99%) were cold-pressed into a disk under the pressure of 20.0 MPa. The as-fabricated disk (Φ60.0 mm × 4.5 mm) was used as the target during sputtering. The *n*-/*p*-GaAs substrates were used in our experiments, respectively. Before the deposition, the substrates were ultrasonically cleaned in sequence by alcohol, acetone, and de-ionized water. Subsequently, MoS_2 thin films with different thickness (d_{MoS2} = ~ 10, 30, 50, 90 nm) were grown on the GaAs substrates at the temperature of 400 °C, respectively. During the deposition, the working pressure and power were kept at 1.0 Pa and 10.0 W, respectively. As a reference, MoS_2 thin films were also deposited on intrinsic GaAs (*i*-GaAs) substrates under the same condition. Finally, about 300-μm In pads with a diameter of 0.5 mm as electrodes were pressed on the MoS_2 film.

The MoS_2 films were characterized using Raman spectroscopy (HORIBA, HR800) with the excitation wavelength of 488 nm. The surface of the sample was scanned by an atomic force microscope (AFM). X-ray photoemission spectroscopy (XPS) was performed by a Kratos Axis ULTRA spectrometer with a monochromatic Al Kα X-ray source. The deposition rate was obtained by the thickness from the cross-sectional scanning electron microscope (SEM) (Additional file 1: Figure S1) and the deposition time, then each film thickness was determined by the deposition rate and each deposition time. The transmission spectra were measured by Shimadzu UV-3150 spectrophotometer. Ultraviolet photoelectron spectroscopy (UPS) was performed using an unfiltered He-I (21.22 eV) gas discharge lamp. LPVs were measured using a Keithley 2000 voltmeter and three-dimensional electric motorized stage with a laser of 650-nm wavelength as the illumination source. The current-voltage (*I*-*V*) curves were measured with a Keithley 2400 SourceMeter.

Results and Discussion

Figure 1 shows the Raman spectrum of the MoS_2 film on the GaAs substrate. Besides the peak of the GaAs substrate at ~ 287.1 cm^{-1}, two characteristic MoS_2 Raman peaks can be seen, the A_{1g} mode at ~ 406.7 cm^{-1} and E^1_{2g} mode at ~ 378.9 cm^{-1}. The right two insets show the illustration of the atomic vibration in MoS_2. The A_{1g} mode corresponds to the S atoms oscillating in antiphase along the out-of-plane direction, and the E^1_{2g} mode corresponds to the S and Mo atoms oscillating in antiphase parallel to the crystal plane. As shown in the figure, the Raman peak corresponding to the A_{1g} mode is preferentially excited for the film. According to our measurements, the intensity ratio of A_{1g}/E^1_{2g} is about 2.1. These Raman characteristics are similar with other reported results about MoS_2 thin films [19]. The left inset shows an AFM topographic image of the 40-nm MoS_2 film grown on the GaAs substrate. From the figure, we can see that the surface of the film is composed of dense cone-like grains. According to the measurements, the root-mean-square (RMS) roughness of

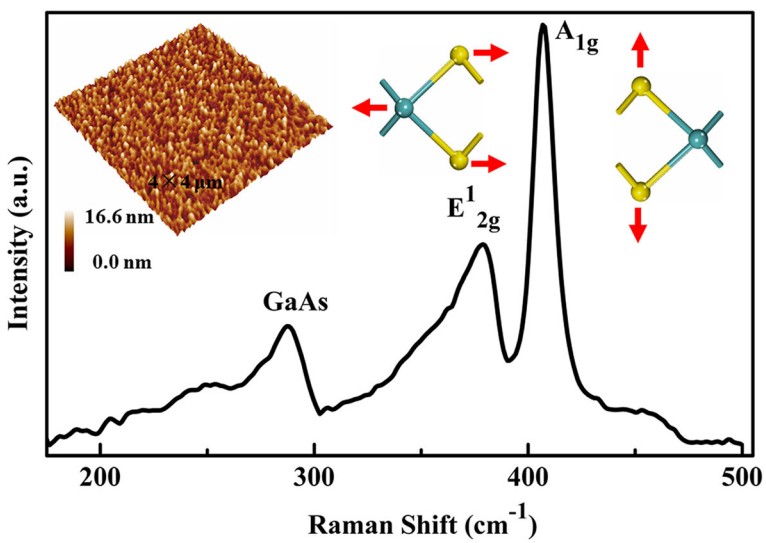

Fig. 1 Raman spectrum of the MoS_2 film on GaAs. The right two insets show the schematic illustrations of the oscillating mode of E^1_{2g} and A_{1g}, respectively. Atom color code: light blue-green, Mo; yellow, S. The left inset shows the surface morphology image of the as-grown MoS_2 films

the film is about 1.7 nm, and the average size of grains is about 76.3 nm in diameter. These grains on the surface could decrease the surface reflection to the external light and enhance the light absorption of the fabricated device.

Figure 2 shows the XPS spectra of the MoS_2 film. As shown in Fig. 2a, the peaks at 229.3 and 232.5 eV are related to the Mo $3d_{5/2}$ and Mo $3d_{3/2}$ orbitals, respectively. As shown in Fig. 2b, S $2p_{3/2}$ and S $2p_{1/2}$ orbitals of divalent sulfide ions (S^{2-}) are observed at 162.2 and 163.3 eV, respectively. The results are in good agreement with the reported values for the MoS_2 crystal [17, 18].

Figure 3a shows the longitudinal *I-V* curve of the fabricated MoS_2/*n*-GaAs heterojunctions. Two In electrodes with the diameter of about 0.5 mm were pressed on the surface of the MoS_2 film and the backside of the GaAs, respectively. The inset shows the schematic circuit for the longitudinal measurements. The forward voltage is defined as a positive bias voltage applied on the top In electrode. As shown in the figure, the fabricated MoS_2/*n*-GaAs heterojunction shows obvious rectifying behaviour. The rectifying ratio (I_+/I_-) measured at ± 1.0 V is about 520. In our experiments, both In/MoS_2 and In/GaAs belong to ohmic contacts and their *I-V* curves are almost linear. Thus, the rectifying *I-V* characteristic in the heterojunction is mainly originated from the MoS_2/GaAs contact. Figure 3b shows the transverse *I-V* curve of the fabricated MoS_2/*n*-GaAs heterojunctions. Two In electrodes with the diameter of about 0.5 mm were pressed on the surface of the MoS_2 film. The top inset shows the schematic circuit for the transverse measurements. From the figure, the *I-V* curve shows slightly nonlinear increase of the currents with increasing voltages. This indicates that an inversion layer at the MoS_2/*n*-GaAs interface is formed [18]. The bottom inset shows the *I-V* curves of the single MoS_2 films on the intrinsic GaAs substrate. From the figure, an almost linear *I-V* curve can be seen, further indicating the ohmic nature of the In/MoS_2 contact. At the voltage of + 0.5 V, the current of the single MoS_2 is about 3.1×10^{-2} μA, much smaller than the value in the MoS_2/*n*-GaAs, about 2.3 μA. Thus, compared to the MoS_2 film, the inversion layer at the MoS_2/*n*-GaAs interface supplies a path with a much lower resistivity for carrier transport during the transverse measurements of the MoS_2/*n*-GaAs heterojunction.

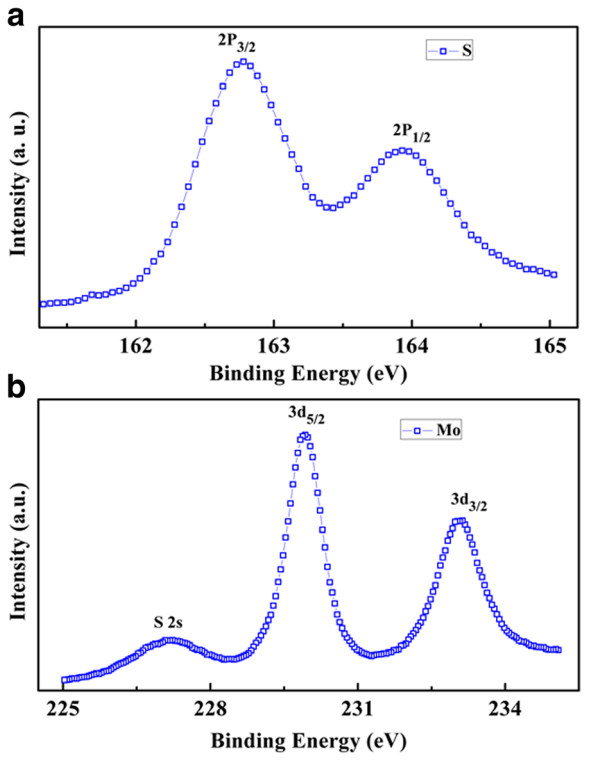

Fig. 2 XPS spectra of the MoS_2 film for **a** Mo and **b** S elements, respectively

Figure 4a shows the schematic circuit for the measurement of the LPE of the fabricated MoS_2/GaAs heterojunction. Two In electrodes with the diameter of 0.5 mm are pressed on the surface of the MoS_2 film to perform the measurements of the LPE. The distance ($2L$) between the electrodes is ~ 1.0 mm. During our measurements, electrodes A and B were connected to the positive and negative probes of a Keithley 2000 voltmeter, respectively. Figure 4b shows the LPE curves of the MoS_2/*n*-GaAs and MoS_2/*p*-GaAs heterojunctions, respectively. The thickness of the MoS_2 films is ~ 30.0 nm. When the surface of the MoS_2 film is partially illuminated by a laser spot with the diameter of about 0.1 mm, a large LPE can be observed in the MoS_2/*n*-GaAs heterojunction. As shown in the figure, the LPE shows an approximately linear dependence on the laser spot position when the laser spot moves between electrodes A and B on the MoS_2 surface. From the figure, we can see that the LPV depends on the position of the laser spot. This can be fitted with the diffusion theory [16],

$$\mathrm{LPV} = K_0\left[\exp\left(-\frac{|L-x|}{d}\right) - \exp\left(-\frac{|L+x|}{d}\right)\right]$$

where K_0, $2L$, d, and x represent a proportionality coefficient, the distance between two electrodes, the carrier diffusion length, and the laser spot position, respectively. The well-fitted results in the figure clearly suggest that the LPE in the MoS_2/*n*-GaAs heterojunction arises from the lateral diffuse flow and recombination of the excited carriers away from the laser position. As shown in the figure, the LPV value is zero when the light spot is at the centre between two electrodes, which can be attributed to the diffusion symmetry of the carriers. When the light

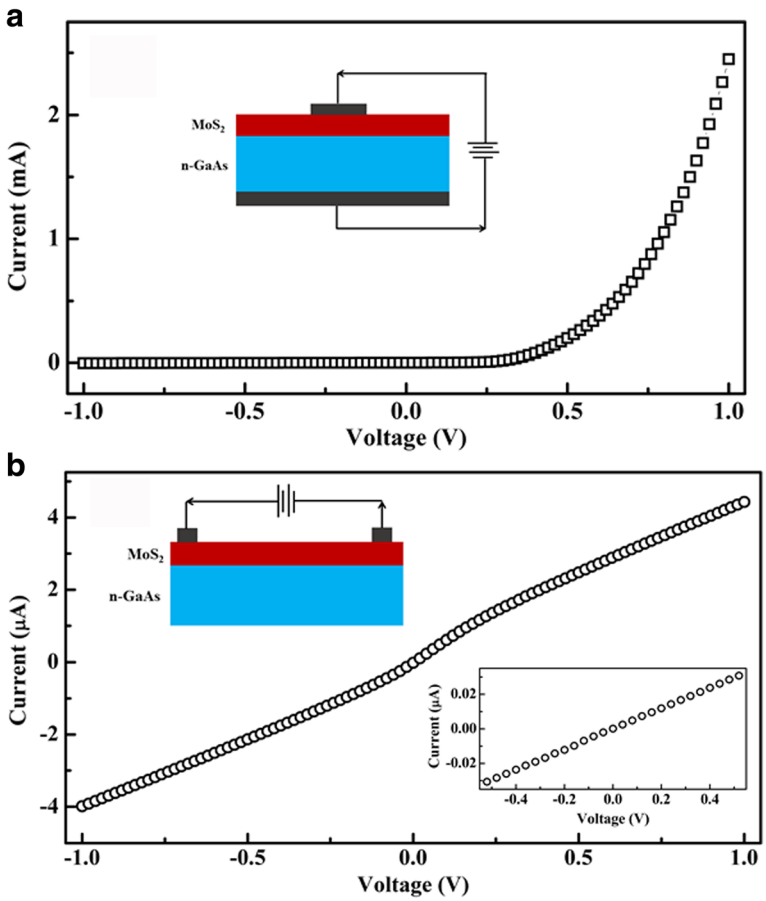

Fig. 3 **a** Longitudinal *I-V* curve of the fabricated MoS_2/*n*-GaAs heterojunctions. The inset shows the schematic circuit for the longitudinal measurements. **b** Transverse *I-V* curves of the fabricated MoS_2/*n*-GaAs heterojunctions. The top inset shows the schematic circuit for the transverse measurements. The bottom inset shows the *I-V* curves of the MoS_2 films on the intrinsic GaAs substrate

position is close to the A electrode, the LPV is positive and vice versa. This indicates that the LPE in the MoS_2/*n*-GaAs heterojunction is caused by the hole-type photoexcited carriers. The maximum LPV is obtained when the laser illumination is closest to the electrodes. According to our measurements, the maximum lateral photovoltage (LPV_{max}) is about 208.2 mV in the linear region of the MoS_2/*n*-GaAs heterojunction. Comparatively, the LPV of the MoS_2/*p*-GaAs heterojunction is much smaller and its LPV_{max} is only 7.3 mV, as shown in the figure. From the figure, we can see that the LPE of the MoS_2/*p*-GaAs heterojunction is determined by the electron-type photoexcited carriers. Additionally, nonlinear LPE characteristics of the MoS_2/*p*-GaAs heterojunction can be seen from the figure when the laser spot moves between the A and B electrodes.

Figure 5 shows the LPE sensitivity of the MoS_2/*n*-GaAs heterojunction as a function of the laser power and the thickness (d_{MoS2}) of the MoS_2 film. The sensitivity is defined by $S = LPV_{max}/L$. Obviously, the S increases drastically with increasing laser power initially but then slowly saturates when the power further increases. This saturation could be caused by the rapidly increasing recombination rate of the photoexcited holes with increasing laser intensity in the illuminated region [20]. As shown in the figure, an obvious LPE and a high sensitivity can be obtained even under the weak laser illumination of 100.0 μW. From the figure, a significant dependence of the sensitivity on the thickness of the MoS_2 films can be seen. When $d_{MoS2} = \sim 10.0$ nm, $S = 165.4$ mV mm^{-1} under the laser illumination of 100.0 μW. With increasing film thickness, S increases gradually. When $d_{MoS2} = 30.0$ nm, S reaches 416.4 mV mm^{-1}. This sensitivity is much larger than the reported MoS_2/Si devices [17, 18]. After $d_{MoS2} > 30.0$ nm, S decreases with further increasing MoS_2 thickness. When $d_{MoS2} = 90.0$ nm, $S = 283.3$ mV mm^{-1}. Thus, to obtain the largest LPE and sensitivity, there is an optimum thickness of the MoS_2 film in the fabricated MoS_2/*n*-GaAs, about 30.0 nm.

Figure 6a presents the UPS spectra of the MoS_2 film on the Si substrate. The work function (W) of the film

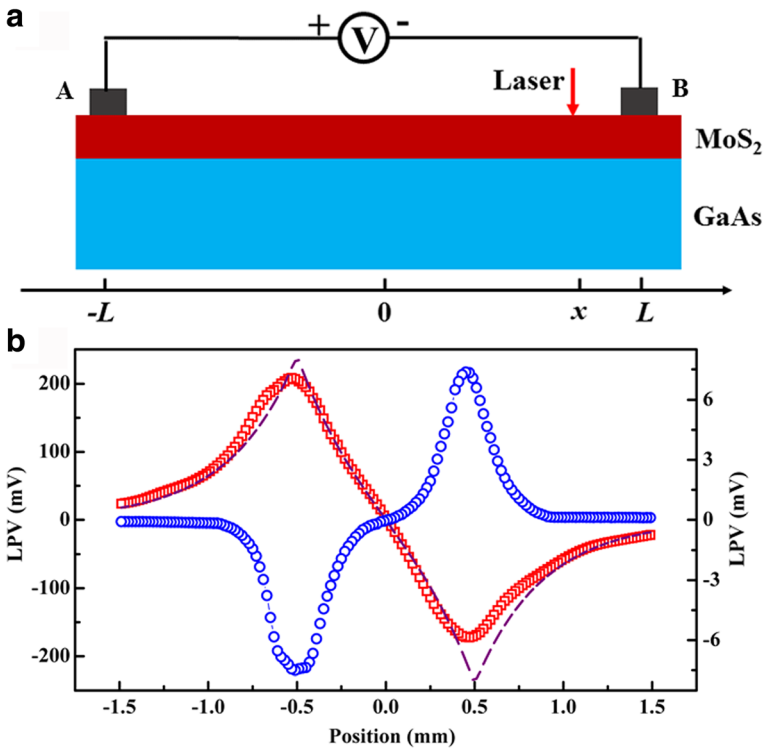

Fig. 4 **a** Schematic circuit for the measurement of the LPE. **b** LPE curves of the MoS_2/*n*-GaAs and MoS_2/*p*-GaAs heterojunctions, respectively

can be calculated from the difference between the cut-off of the highest binding energy and the photon energy of the exciting radiation. From the figure, W = 5.24 eV can be obtained. The distance (ΔE) between the valence band (E_V) and the Fermi level (E_F) of MoS_2 film can be extracted from the onset energy, as shown in the inset. The ΔE for the MoS_2 film is about 0.51 eV. Using the data from the transmittance spectrum of the MoS_2 film on quartz substrate, $(\alpha h\nu)^2$ is plotted as a function of photon energy $h\nu$, wherein h is the Planck constant and ν is the photon frequency. The α is the absorption coefficient, calculated by $\alpha d = \ln(1/T)$ [21], wherein d and T are the thickness and transmittance of the film, respectively. The band gap (E_g) of the film can be determined

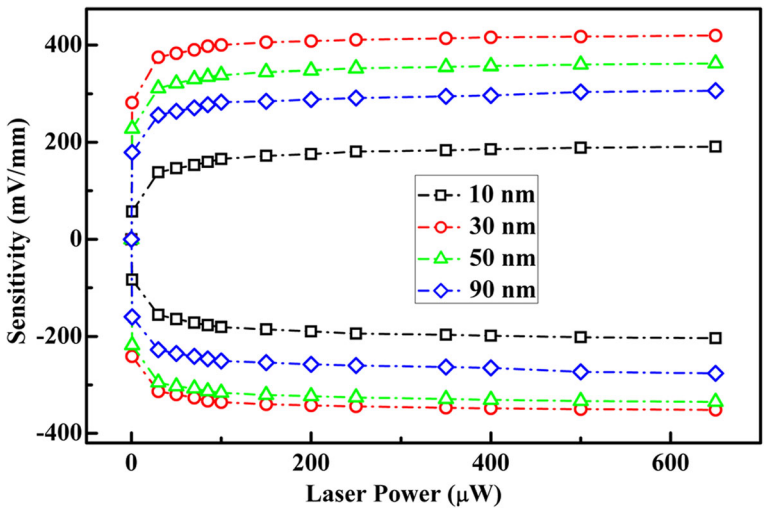

Fig. 5 Dependence of positive and negative sensitivities of the fabricated MoS_2/*n*-GaAs heterojunction on laser powers, respectively

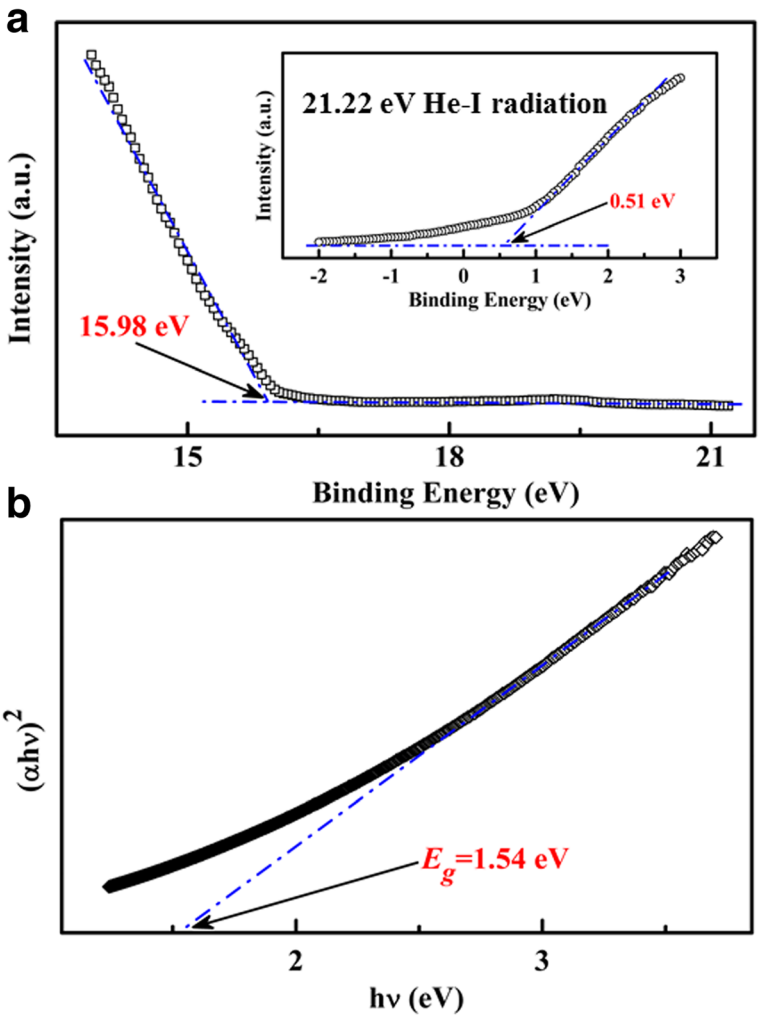

Fig. 6 a UPS spectra of the MoS_2 film on GaAs, showing the Fermi level of the films and the distance between the Fermi level and the top edge of the conduction band. **b** $(ahv)^2$~hv curve from UV spectrum of the MoS_2 film on quartz substrate under the same deposition condition

from the intercept of the line on the $h\nu$ axis, E_g = 1.54 eV, as shown in Fig. 6b. Based on these energy-band parameters, the p-type behaviour of the MoS_2 film can be determined, which can be further proved by Hall measurements. The Hall results show that the concentration of the hole-type carrier and the mobility are about 3.8×10^{15} cm^{-3} and 11.2 cm^2 V^{-1} s^{-1}, respectively.

In order to clarify the mechanisms of the LPE in the MoS_2/GaAs heterojunctions, the energy-band diagrams at the interface are constructed based on the results in Fig. 6. Here, E_g = 1.42 eV and E_F = 4.17 eV for n-GaAs are taken into account to construct the band structure [22]. When the MoS_2 film is deposited onto the GaAs substrate, the electrons flow from the GaAs into the MoS_2 film at the interface due to the higher E_F of the GaAs. The flowing process stops when Fermi levels are equal and the MoS_2/GaAs p-n junction is fabricated, as shown in Fig. 7a. Consequently, a built-in field (E_{bi}) is formed at the interface of the MoS_2/GaAs heterojunction. $E_{bi} = [E_F(n\text{-GaAs}) - E_F(MoS_2)]/e$ = 1.07 V and it points from the GaAs to the MoS_2 film. Thus, the asymmetric longitudinal I-V curve is shown in Fig. 3a. Due to the existence of a strong E_{bi}, large quantities of hole-type carriers are accumulated near the interface and an inversion layer is formed in the n-GaAs substrate near the interface, as shown in Fig. 7b. Similar with the two-dimensional hole gas (2DHG) [23], the inversion layer could exhibit the feature of high conduction due to the high sheet concentration of the holes (p+). From Fig. 3b, we can see that the conduction of the inversion layer is much larger than the MoS_2 film. Thus, the conduction between two electrodes on the same side of the MoS_2 film is dominated by the inversion layer rather than the MoS_2 film. When the junction is partially illuminated by the laser, the light is absorbed and the electron-hole

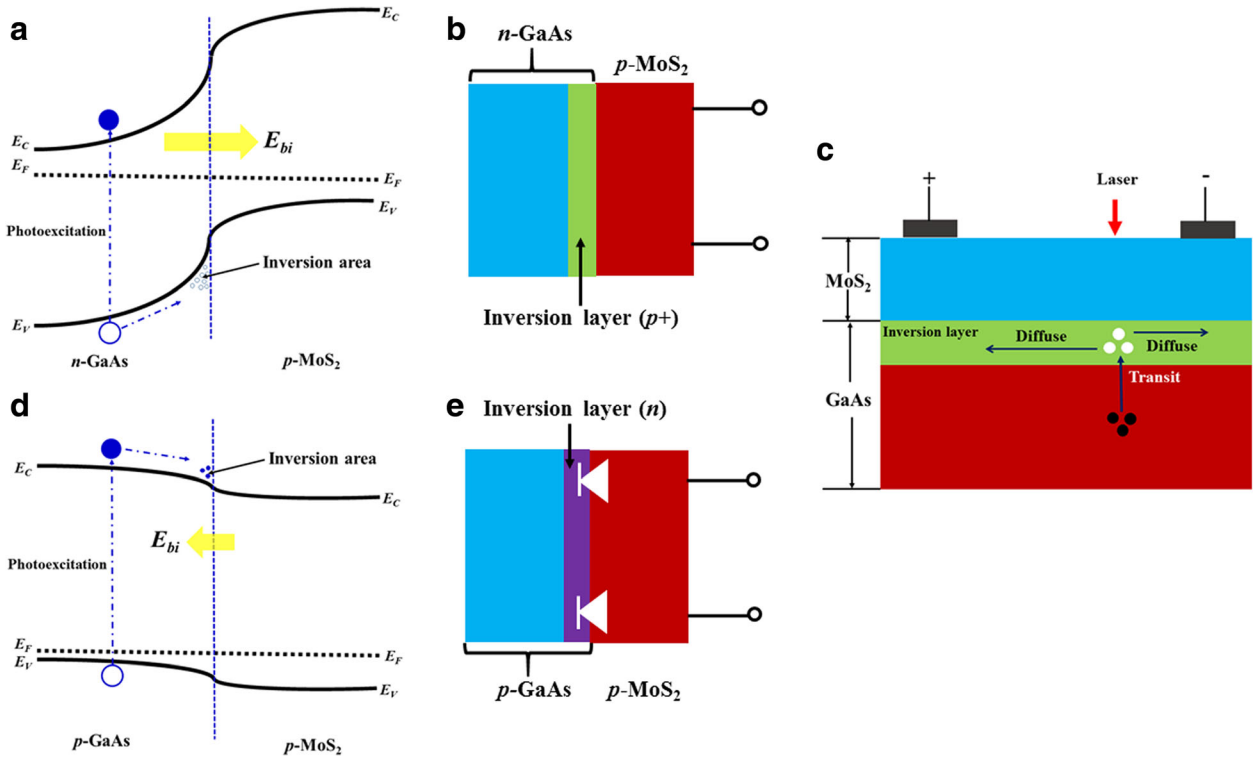

Fig. 7 **a** Energy-band alignment of the MoS_2/*n*-GaAs heterojunction, and **b** the corresponding illustration of the electrical contacting at the interface. **c** Mechanism of the LPE in the MoS_2/*n*-GaAs heterojunction. **d** Energy-band alignment of the MoS_2/*p*-GaAs heterojunction, and **e** the corresponding illustration of the electrical contacting at the interface

pairs in the MoS_2 film and GaAs can be induced, respectively, as shown in Fig. 7c. However, it can be expected that most of the laser is absorbed by the GaAs substrates due to its much larger thickness and smaller band gap. Under the laser illumination, the electron-hole pairs can only be excited in the illuminated region and spatially separated by the E_{bi}. Due to the orientation of the E_{bi} pointing from GaAs to MoS_2, the photoexcited holes flow towards the interface and enter into the inversion layer in the GaAs, as shown in Fig. 7c. The photoexcited holes in the inversion layer diffuse laterally away from the illuminated spot to the two electrodes. The concentration of the excited holes collected by the two electrodes is different for different distances from the illuminated spot. Thus, a large LPV is formed between the electrodes, and the LPE is observed in the heterojunction. This is in accord with the fitted results from Fig. 3b, and the LPE in the MoS2/*n*-GaAs heterojunctions mainly originates from the carrier diffusion. When the MoS_2 film is deposited onto the *p*-GaAs substrate, a *p-p* heterojunction is formed, as shown in Fig. 7d. E_F(*p*-GaAs) = 5.32 eV is used in the band diagram [22]. The E_{bi} of the *p-p* heterojunction can be calculated, 0.08 V, and its direction points from the film to the substrate. Due to the E_{bi}, electron-type carriers are accumulated near the interface of the heterojunction and the inversion layer is formed. Thus, the LPE induced by the diffusion of the photoexcited electrons is obtained in the MoS_2/GaAs *p-p* heterojunction, as shown in Fig. 4. However, the concentration of the accumulated carrier in the inversion layer might be lower due to the weak V_{bi} of only 0.08 V in the *p-p* heterojunction compared to the *p*-MoS_2/*n*-GaAs junction. This increases the difficulties of the transport of the photoexcited electrons in the inversion layer. Seriously, the Schottky barriers can be formed between the *n*-type inversion layer and the *p*-MoS_2 film, as shown in Fig. 7e. These characteristics of the *p*-MoS_2/*p*-GaAs junction suppress the collection of the photoexcited electrons at the electrodes. As a result, the LPE could be reduced largely. As shown in Fig. 4b, the LPV_{max} for the *p-p* junction is only 7.3 mV while it reaches 208.2 mV in the *p-n* junction.

It usually happens in the reported heterojunction-type PSDs that the LPE can be tuned by changing the thickness of the cap layers [20]. This can be well understood by considering the recombination of the photoexcited carriers in the film and the evolution of the built-in field. In the MoS_2/GaAs *p-n* junction, the recombination of photon-generated carriers can be enhanced due to the long transporting path in the thick MoS_2 film before

they are collected by the electrodes. This reduces the LPE of the heterojunctions. Reversely, a thinner film can greatly decrease the recombination, which causes the increase of the LPE. However, when the MoS_2 thickness is smaller than the critical value, the E_{bi} at the interface decreases with further decreasing MoS_2 thickness [24]. This can reduce the separation of photon-generated electron-hole pairs, and the LPE decreases. Thus, there is an optimum thickness of the MoS_2 film for obtaining the highest LPE, about 30 nm.

Conclusions

In summary, MoS_2 thin films were deposited on the surface of the GaAs substrate via magnetron sputtering technique. A large LPE was obtained in the fabricated MoS_2/*n*-GaAs heterojunction, and the dependence of the LPV on the position of the laser illumination showed good linearity. Due to the formation of the strong built-in field at the interface, the MoS_2/*n*-GaAs heterojunction exhibited a high sensitivity of 416.4 mV mm^{-1}, while the value was only 7.3 mV mm^{-1} for the MoS_2/*p*-GaAs. Our results further showed that the LPE exhibited obvious dependence on the thickness of the MoS_2 films and about 30.0 nm was the optimum thickness of the MoS_2 film to acquire the highest LPE in the fabricated MoS_2/*n*-GaAs heterojunctions. The mechanisms to the LPE in the MoS_2/GaAs devices were clarified based on the energy-band alignment at the interface.

Additional file

Additional file 1: Large lateral photovoltaic effect in MoS_2/GaAs heterojunction. Figure S1. Cross-sectional SEM images of the as-grown MoS_2 film. (DOCX 731 kb)

Abbreviations

ΔE: Distance between E_V and E_F; d_{MoS2}: Thickness of the MoS_2 film; E_{bi}: Built-in field; E_C: Conduction band level; E_F: Fermi energy level; E_g: Energy-band gap; E_V: Valence band level; *I-V*: Current-voltage; LPE: Lateral photovoltaic effect; LPV: Lateral photovoltage; LPV_{max}: Maximum lateral photovoltage; MoS_2: Molybdenum disulfide; PSD: Position-sensitive detector; UPS: Ultraviolet photoelectron spectroscopy; *W*: Work function

Acknowledgements

This work was supported by the financial support by the National Natural Science Foundation of China (51502348), Shandong Natural Science Foundation (ZR2016AM15), Open Foundation of State Key Laboratory of Electronic Thin Films and Integrated Devices (KFJJ201606), and Fundamental Research Funds for the Central Universities (15CX08009A).

Funding

The National Natural Science Foundation of China (51502348), Shandong Natural Science Foundation (ZR2016AM15), and Open Foundation of State Key Laboratory of Electronic Thin Films and Integrated Devices (KFJJ201606) act as guide to the design of the study and the collection, analysis, and interpretation of the data and the publication of the study.

Authors' Contributions

LH participated in the fabrication of MoS_2/GaAs heterojunctions, analysed the data, and wrote the manuscript. YL interpreted the data for Raman spectrum. ZH performed the electrical measurements. ZX participated in the construction of the energy-band diagram. JZ discussed the mechanisms of the LPE. All authors read and approved the final manuscript.

Authors' Information

LH is an associate professor in materials physics and PhD degree holder specializing in electronic thin films and integrated devices. YL is an associate professor and PhD degree holder in the growth of thin films. ZH is a lecturer studying on optical-electronic materials and optoelectronic devices. ZX is a lecturer studying on composited materials. JZ is a professor and PhD degree holder specializing in physical vapour deposition technique.

Ethics Approval and Consent to Participate

Not applicable.

Consent for Publication

Not applicable.

Competing Interests

The authors declare that they have no competing interests.

Publisher's Note

Received: 8 August 2017 Accepted: 30 September 2017
Published online: 10 October 2017

References

1. Jariwala D, Sangwan VK, Lauhon LJ, Marks TJ, Hersam MC (2014) Emerging device applications for semiconducting two-dimensional transition metal dichalcogenides. ACS Nano 8:1102–1120
2. Zheng B, Chen Y, Wang Z, Qi F, Huang Z, Hao X, Li P, Zhang W, Li Y (2016) Vertically oriented few-layered HfS2 nanosheets: growth mechanism and optical properties. 2D Mater 3:035024
3. Zheng B, Chen YF, Qi F, Wang XQ, Zhang WL, Li YR, Li XS (2017) 3D-hierarchical MoSe2 nanoarchitecture as a highly efficient electrocatalyst for hydrogen evolution. 2D Mater 4:025092
4. He J, Li P, Lv W, Wen K, Chen YF, Zhang WL, Li YR, Qin W, He W (2016) Three-dimensional hierarchically structured aerogels constructed with layered MoS_2/graphene nanosheets as free-standing anodes for high-performance lithium ion batteries. Electrochim Acta 215:12–18
5. Qi F, Li P, Chen YF, Zheng B, Liu XZ, Lan F, Lai Z, Xu Y, Liu J, Zhou J, He J, Zhang WL (2015) Effect of hydrogen on the growth of MoS_2 thin layers by thermal decomposition method. Vacuum 119:204–208
6. Mak KF, Lee C, Hone J, Shan J, Heinz TF (2010) Atomically thin MoS_2: a new direct-gap semiconductor. Phys Rev Lett 105:136805
7. Radisavljevic B, Radenovic A, Brivio J, Giacometti V, Kis A (2011) Single-layer MoS_2 transistors. Nat Nanotech 6:147–150
8. Yin Z, Li H, Li H, Jiang L, Shi Y, Sun Y, Lu G (2010) Single-layer MoS_2 phototransistors. ACS Nano 6:74–80
9. Lin S, Li X, Wang P, Xu Z, Zhang S, Zhong H, Wu Z, Xu W, Chen H (2015) Interface designed MoS_2/GaAs heterostructure solar cell with sandwich stacked hexagonal boron nitride. Sci Rep 5:15103
10. Xu Z, Lin S, Li X, Zhang S, Wu Z, Xu W, Lu Y, Xu S (2016) Monolayer MoS_2/GaAs heterostructure self-driven photodetector with extremely high detectivity. Nano Energy 3:89–96
11. Wang L, Jie J, Shao Z, Zhang Q, Zhang X, Wang Y, Sun Z, Lee ST (2015) MoS_2/Si heterojunction with vertically standing layered structure for ultrafast, high-detectivity, self-driven visible-near infrared photodetectors. Adv Func Mater 25:2910–2919
12. Pradhan SK, Xiao B, Pradhan AK (2016) Enhanced photo-response in *p*-Si/MoS_2 heterojunction-based solar cells. Sol Energy Mater Sol Cells 144:117–127
13. Ruzmetov D, Zhang K, Stan G, Kalanyan B, Bhimanapati GR, Eichfeld SM, Burke RA, Shah PB, O'Regan TP, Crowne FJ, Glen BA, Robinson JA, Davydov AV, Ivanov TG (2016) Vertical 2D/3D semiconductor heterostructures based on epitaxial molybdenum disulfide and gallium nitride. ACS Nano 10:3580–3588

14. Yu CQ, Wang H, Xia YX (2009) Giant lateral photovoltaic effect observed in TiO_2 dusted metal-semiconductor structure of Ti/TiO_2/Si. Appl Phys Lett 95:141112
15. Yu CQ, Wang H, Xiao SQ, Xia YX (2009) Direct observation of lateral photovoltaic effect in nano-metal-films. Opt Express 17:21712–21722
16. Liu S, Xie X, Wang H (2014) Lateral photovoltaic effect and electron transport observed in Cr nano-film. Opt Express 22:11627–11632
17. Qiao S, Zhang B, Feng K, Cong R, Yu W, Fu G, Wang S (2017) Large lateral photovoltage observed in MoS_2 thickness-modulated ITO/MoS_2/*p*-Si heterojunctions. ACS Appl Mater Interfaces 9:18377–18387
18. Hu C, Wang X, Miao P, Zhang L, Song B, Liu W, Lv Z, Zhang Y, Sui Y, Tang J, Yang Y, Song B, Xu P (2017) Origin of the ultrafast response of the lateral photovoltaic effect in amorphous MoS_2/Si junctions. ACS Appl Mater Interfaces 9:18362–18368
19. Late DJ, Shaikh PA, Khare R, Kashid RV, Chaudhary M, More MA, Ogale SB (2014) Pulsed laser-deposited MoS_2 thin films on W and Si: field emission and photoresponse studies. ACS Appl Mater Interfaces 6:15881–15888
20. Wang X, Zhao X, Hu C, Zhang Y, Song B, Zhang L, Liu W, Lv Z, Zhang Y, Tang J, Sui Y, Song B (2016) Large lateral photovoltaic effect with ultrafast relaxation time in SnSe/Si junction. Appl Phys Lett 109:023502
21. Chen X, Ruan K, Wu G, Bao D (2008) Tuning electrical properties of transparent *p*-NiO/*n*-MgZnO/*p*-NiO/*n*-MgZnO heterojunctions with band gap engineering of MgZnO. Appl Phys Lett 93:112112
22. Liu EK, Zhu BS, Luo JS (eds) (2011) The physics of semiconductors. Electronic Industry, Beijing, pp p191–p195
23. Kawarada H, Yamada T, Xu D, Tsuboi H, Kitabayashi Y, Matsumura D, Shibata M, Kudo T, Inaba M, Hiraiwa A (2017) Durability-enhanced two-dimensional hole gas of C-H diamond surface for complementary power inverter applications. Sci Rep 7:42368
24. Zhao K, Jin KJ, Lu H, Huang Y, Zhou Q, He M, Chen Z, Zhou Y, Yang G (2006) Transient lateral photovoltaic effect in p-n heterojunctions of $La_{0.7}Sr_{0.3}MnO_3$ and Si. Appl Phys Lett 88:141914